

**ENHANCING SOFTWARE QUALITY: A NOVEL  
APPROACH TO BUG LOCALIZATION USING HYBRID AI  
TECHNIQUES**

**Muhammad Zahid**

*Department of Mathematics and statistics, Institute of Southern Punjab, Multan, Pakistan*

[muhammadzahid82@gmail.com](mailto:muhammadzahid82@gmail.com)

**M Rashid Iqbal**

*Department of Mathematics and statistics, Institute of Southern Punjab, Multan, Pakistan*

[rashidiqbalkhan554@gmail.com](mailto:rashidiqbalkhan554@gmail.com)

DOI: <https://doi.org/10.71146/kjmr157>

**Article Info**



**Abstract**

*This research examines the aerodynamic behavior of a NACA 0012 airfoil under subsonic flow conditions. The behavior is examined in terms of the lift which is produced as a result of air attacking the airfoil. Lift coefficient is calculated against angle of attack for different inlet velocity conditions using a C-type geometry. The mathematical model comprises the Nervier-Stokes equations along with the Standard k- $\epsilon$  turbulence model to capture the turbulence. The mathematical model is a set of nonlinear partial differential equations to be solved simultaneously. We used the finite volume method to solve our problem. All tasks of simulations are accomplished using ANSYS Workbench 16.2.*



This article is an open access article distributed under the terms and conditions of the Creative Commons Attribution (CC BY) license  
<https://creativecommons.org/licenses/by/4.0/>

**Keywords:** NACA 0012 airfoil, angle of attack, Lift coefficient, Drag coefficient, CFD

## Introduction

An airfoil, featuring a curved upper surface and a flatter lower surface, or curved on both the upper and lower sides which may be symmetric or nonsymmetrical, is a specially designed shape used in aircraft wings, blades, and other applications. It generates lift by exploiting the difference in air pressure created when air flows over its surfaces. This pressure disparity enables aircraft to fly and stay aloft. It is designed very carefully to present the desired lift characteristics, allowing the body to gain resistance and reducing the need for extra thrust thereby enhancing overall aerodynamic performances. The NACA 0012 airfoil stands out for its symmetrical upper and lower surfaces, ensuring equal airflow on both sides. This symmetry simplifies its construction and enhances its flying stability, making it ideal for various aircrafts from general aviation to fast jets. It is precisely engineered shape that reduces drag at varying speeds while generating the necessary lift. Maintaining this balance is crucial for maintaining stable and safe flight operations.

Research by Basha [1] compared mesh configurations for NACA 0012 airfoil simulations. Results showed the hybrid mesh, featuring enhanced boundary layer resolution, yielded improved drag coefficient predictions. Stuck et al. [2] opted for a combined mesh comprising quadrilateral unstructured cells to facilitate seamless transitions from the boundary layer mesh to the outer mesh for Reynolds Averaged Navier Stokes (RANS) simulations on a rudder profile. To ensure grid independence, parametric studies were conducted, systematically varying chord-wise and layer-wise grid refinements, and selecting optimal parameters based on integral force coefficient fluctuations. Turnock et al. [3] conducted an in-depth investigation on the NACA 0012 airfoil, focusing on the independent effects of boundary location and mesh node distribution patterns. Key parameters were systematically determined through convergence analyses, ensuring optimal spatial resolution. Gawali and Mane [4] conducted a comprehensive investigation combining experimental and the CFD analyses. Their study examined airflow at 15 m/s over an airfoil, exploring angle of attack ( $\alpha$ ) from 0° to 20°. Key

outcomes revealed detailed pressure distribution patterns and lift force dynamics acting on the airfoil. Wenzinger [5] conducted wind tunnel experiments to evaluate the aerodynamic performance of the diverse flap configurations. Notably, the slotted flap design exhibited a significant enhancement in lift coefficient ( $C_L$ ), outperforming other tested flap types. Research conducted by Todorov [6] and Hussein et al. [7] demonstrated that incorporating a slotted flap design into airfoil configurations yields significant enhancements in lift coefficient ( $C_L$ ) and drag coefficient ( $C_D$ ) values through computational simulations. Airfoil theory predicts that integrating a slotted flap into the NACA 0012 design will yield elevated lift coefficients ( $C_L$ ) compared to the baseline configuration, with more pronounced enhancements at increased flap angles. The ( $C_L$ ) slope relative to  $\alpha$  is anticipated to remain relatively consistent. Conversely, the introduction of the flap disrupts the airfoil's streamlined profile, particularly at higher angles, leading to increased drag coefficients ( $C_D$ ). Further ( $C_D$ ) augmentations are expected with larger flap angles. Notably, rising air velocities and corresponding Reynolds numbers should precipitate a marginal decrease in  $C_D$  [8, 9,10]. The developed model must accurately capture the variations in lift coefficient ( $C_L$ ) and drag coefficient ( $C_D$ ) resulting from modifications to airfoil geometry and alterations in free-stream flow conditions. Sogukpinar et al. [11] calculated lift, drag coefficient, lift to drag ratio, and power coefficient at different velocities by simulating airflow over the inclined NACA 632-215 airfoil using the SST turbulence model. Results showed that the lift and drag coefficients are increasing with the wind velocity, while the lift to drag ratio peaked at 4° before decreasing. Conversely, experimental investigations by Mehrdad Ghods [12] on the NACA 2415 airfoil revealed lift coefficient augmentation with  $\alpha$  increments between -5° and 17°, followed by stall-induced drag dominance beyond 17°. Comparing theoretical and experimental data, higher drag coefficients were observed experimentally, attributable to airfoil section imperfections and testing inaccuracies. Rajakumar et al. [13] conducted an in-depth analysis of horizontal-axis wind turbine aerodynamics, focusing on NACA 4410 and 2415

airfoils. Particle image velocimetry (PIV) flow surveys and pressure measurements were coupled with 2D and 3D CFD simulations to verify numerical models [14]. Furthermore, Kiumars Khani Aminjan [15] utilized CFD techniques to analyze lift and drag forces on NACA 2012-65 airfoils across various attacking angles. Hong et al. [16] explored innovative flow control strategies through inflation and suction on NACA 0012 airfoils. Rosas [17] conducted numerical simulations of flow oscillation injection, achieving a remarkable 93% increase in force utilizing composite jets. Belliganor and Labio [18] optimized flow control via evolutionary algorithms. The distinctive wing shape of NACA 0012 airfoils reduces drag, minimizes shock waves and influences aircraft maneuverability and lift capabilities [19].

In the current manuscript, we performed CFD simulation for NACA 0012 airfoil to investigate the lift coefficient, drag coefficient and their ratio against  $\alpha$  for various inlet velocities. Note that the NACA four-digit wing sections define the profile as; the first digit describes maximum camber as percentage of the chord, second digit describes the distance of maximum camber from the airfoil leading edge in tenths of the chord, while the last two digits describe maximum thickness of the airfoil as percent of the chord.

## 1. Problem Statement

In our work, we compute and analyze flow characteristics around NACA 0012 airfoil whose profile is given in Fig. 1. The length of the cross-section of the airfoil is 1 m, while its maximum thickness is 0.12 m. The profile is symmetric about the chord line. The objective is to investigate the lift coefficient, drag coefficient and their ratio against  $\alpha$  for various inlet velocities.

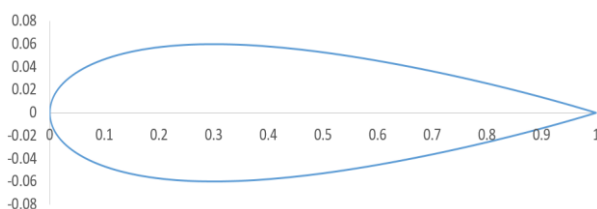


Fig. 1. NACA 0012 airfoil profile

## 1.1 Computational Geometry

The computational domain for computations is a C-type geometry as shown in Fig. 2. The circular arcs on the left side are the velocity inlet while the

vertical line on the right side is the pressure outlet. The horizontal lines attached to the outlet are symmetry lines. The computational domain is the fluid (air) zone only. The airfoil body is a solid body and hence it is not the part of the computational domain, rather it is present as a solid boundary. The length of the airfoil is 1m. We create the computational geometry in ANSYS Design Modeler. The radius of the circular arcs is 3m, the length of the symmetry line is 3m and the length of the outlet is 6m.

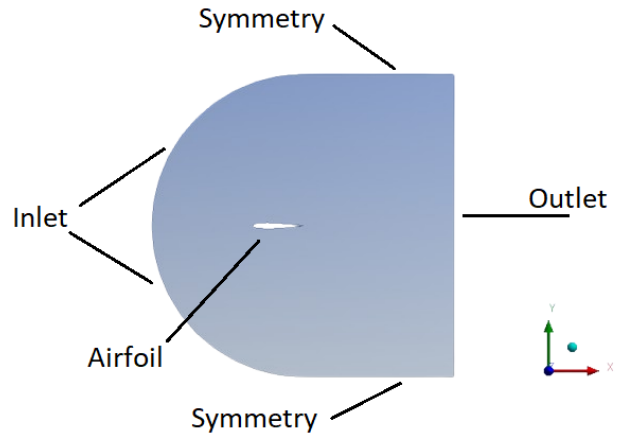


Fig. 2. Computational domain

## 2. Mathematical Model

In this paper discusses the mathematical model, which includes each the flow and the turbulence model. After that, the flow model is solved using the finite volume methods. The model and method will be described in detail in the sections that follow.

### 2.1 Flow Model

The continuity equation for a two-dimensional, steady, and incompressible flow is as follows:

$$\frac{\partial u}{\partial x} + \frac{\partial v}{\partial y} = 0$$

The momentum equations for viscous flow in the x and y directions are as follows:

$$\rho \left( \frac{\partial u}{\partial t} + u \frac{\partial u}{\partial x} + v \frac{\partial u}{\partial y} \right) = - \frac{\partial p}{\partial x} + \rho \delta_x + \mu \left( \frac{\partial^2 u}{\partial x^2} + \frac{\partial^2 u}{\partial y^2} \right)$$

$$\rho \left( \frac{\partial v}{\partial t} + u \frac{\partial v}{\partial x} + v \frac{\partial v}{\partial y} \right) = - \frac{\partial p}{\partial y} + \rho \delta_y + \mu \left( \frac{\partial^2 v}{\partial x^2} + \frac{\partial^2 v}{\partial y^2} \right)$$

### 2.2 Turbulence Model

We use Standard  $k-\epsilon$  turbulence models for capturing the turbulence in the flow. This model contains two transport equations which are simultaneously solved with the flow model. These

equations are

$$\frac{\partial}{\partial t}(\rho k) + \frac{\partial}{\partial x_i}(\rho k \mu_i) = \frac{\partial}{\partial x_i} \left[ \mu + \left( \frac{\mu_t}{\sigma_k} \right) \frac{\partial k}{\partial x_i} \right] + G_k + G_b - \rho \in -Y_M + S_k$$

$$\frac{\partial}{\partial t}(\rho k) + \frac{\partial}{\partial x_i}(\rho \epsilon \mu_i) = \frac{\partial}{\partial x_i} \left[ \mu + \left( \frac{\mu_t}{\sigma_\epsilon} \right) \frac{\partial \epsilon}{\partial x_i} \right] + C_{le} \frac{\epsilon}{k} (G_b) - C_{2e} \rho \frac{\epsilon^2}{k} + S_\epsilon$$

### 2.3 Discretization

We use the finite volume method to solve our flow model. This method discretizes the partial differential equations on each finite volume converting them into system of linear algebraic equations to be solved simultaneously.

### 2.4 Meshing

In order to use the finite volume method, the computational domain must be discretized into smaller volumes. In our computational mesh, there are 2820 nodes and 5286 elements with an average skewness of 0.062032, an average aspect ratio of 1.2167 and an average orthogonal quality of 0.96215. The mesh of the computational domain is shown in Figures 3.

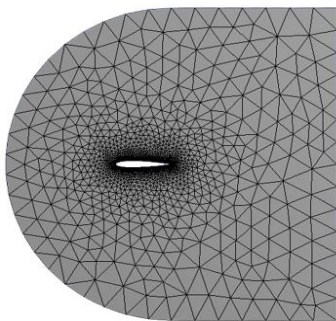


**Fig. 3. Computational Mesh and zoomed view of mesh around the airfoil**

### 2.5 Coefficient of Lift and Coefficient of Drag

The lift coefficient is calculated using the relation given below

$$C_L = \frac{\text{Lift force}}{0.5 \rho V^2 A}$$

The dynamic pressure  $q$  is equal to  $0.5 \rho V^2$ . Hence, the above equation takes the form

$$C_L = \frac{L}{qA}$$

The drag coefficient  $C_D$  is dimensionless measurement used in aerodynamics to quantify the resistance an item faces when travelling through a fluid.  $C_D$  can be calculated by the equation,

$$C_D = \frac{\text{Drag force}}{0.5 \rho V^2 A}$$

The above equation may be written as

$$C_D = \frac{D}{qA}$$

The drag force, a measure of the resistance opposing an object's motion, can be calculated using the formula: Drag Force =  $P \times A \times V$ . In this equation,  $P$  represents the density of the fluid,  $A$  signifies the reference area of the object, and  $V$  denotes the velocity of the object relative to the fluid. This fundamental concept is crucial in understanding the dynamics of fluid motion and its impact on objects moving through it.  $C_D$  = Drag Coefficient.

### 3. Results and Discussion

In the current study, we investigate the impact of the  $\alpha$  and inlet velocity on the coefficient of lift  $C_L$ , coefficient of drag  $C_D$  and their ratio  $C_L/C_D$ . The  $\alpha$  varies from  $0^\circ$  to  $40^\circ$  with a gap of  $2^\circ$ .

In Fig. 4 (a), the  $C_L$  is plotted against  $\alpha$  for an inlet velocity of 2 m/s. We observe that the  $C_L$  increases from 0 to 2.6 linearly against  $\alpha$  from  $0$  to  $14^\circ$ . The  $C_L$  increases further up to 2.8 against  $\alpha=18^\circ$ . On increasing  $\alpha$  further, results in a decrease in  $C_L$ . This behavior continues up to  $24^\circ$ . After this value, the  $C_L$  starts rising again very slowly. The value of  $C_L$  is 2.8 when  $\alpha=40^\circ$ . A similar pattern is observed in the other graphs of Fig. 4, i.e., Fig. 4 (b), (c), (d) and (e).

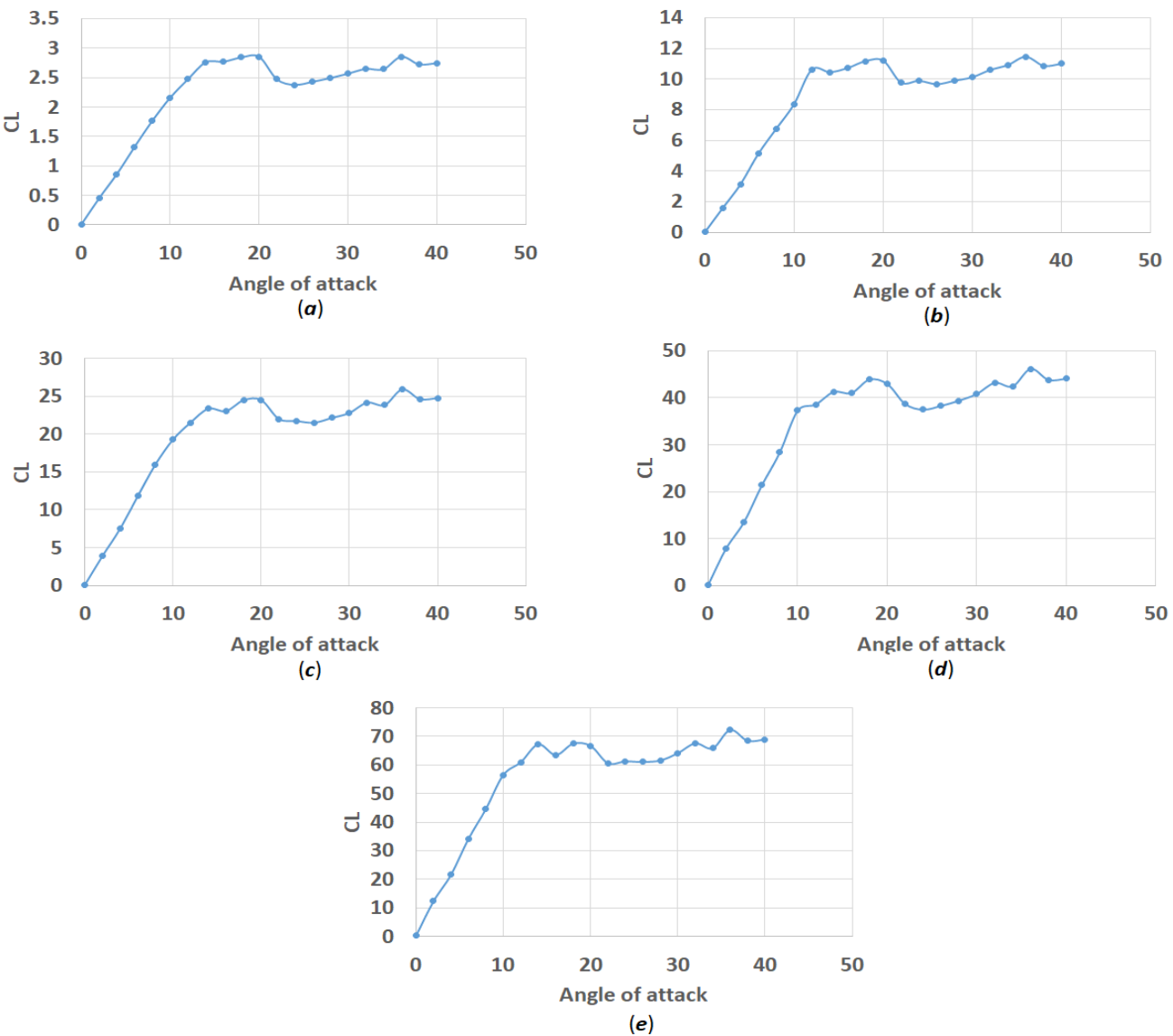


**Fig. 4. Coefficient of lift  $C_L$  against  $\alpha$  for inlet velocity (a)  $u = 2 \text{ m/s}$ , (b)  $u = 4 \text{ m/s}$ , (c)  $u = 6 \text{ m/s}$ , (d)  $u = 8 \text{ m/s}$  and (e)  $u = 10 \text{ m/s}$**

In Fig. 5 (a), we see that the  $C_D$  increases slightly against the  $\alpha$  from  $0^\circ$  to  $8^\circ$ . Then there is rapid rise in the slope of  $C_D$  curve and it continues up to  $18^\circ$   $\alpha$ . After  $\alpha=18^\circ$ , the curve is straightened, i.e., the

slope becomes constant and the  $C_D$  continue rising linearly for rest of the values of  $\alpha$ . The  $C_D$  attains a value of 2.2 at  $\alpha=40^\circ$ . A similar pattern is observed in the other graphs of Fig. 5, i.e., Fig. 5 (b), (c), (d) and (e).

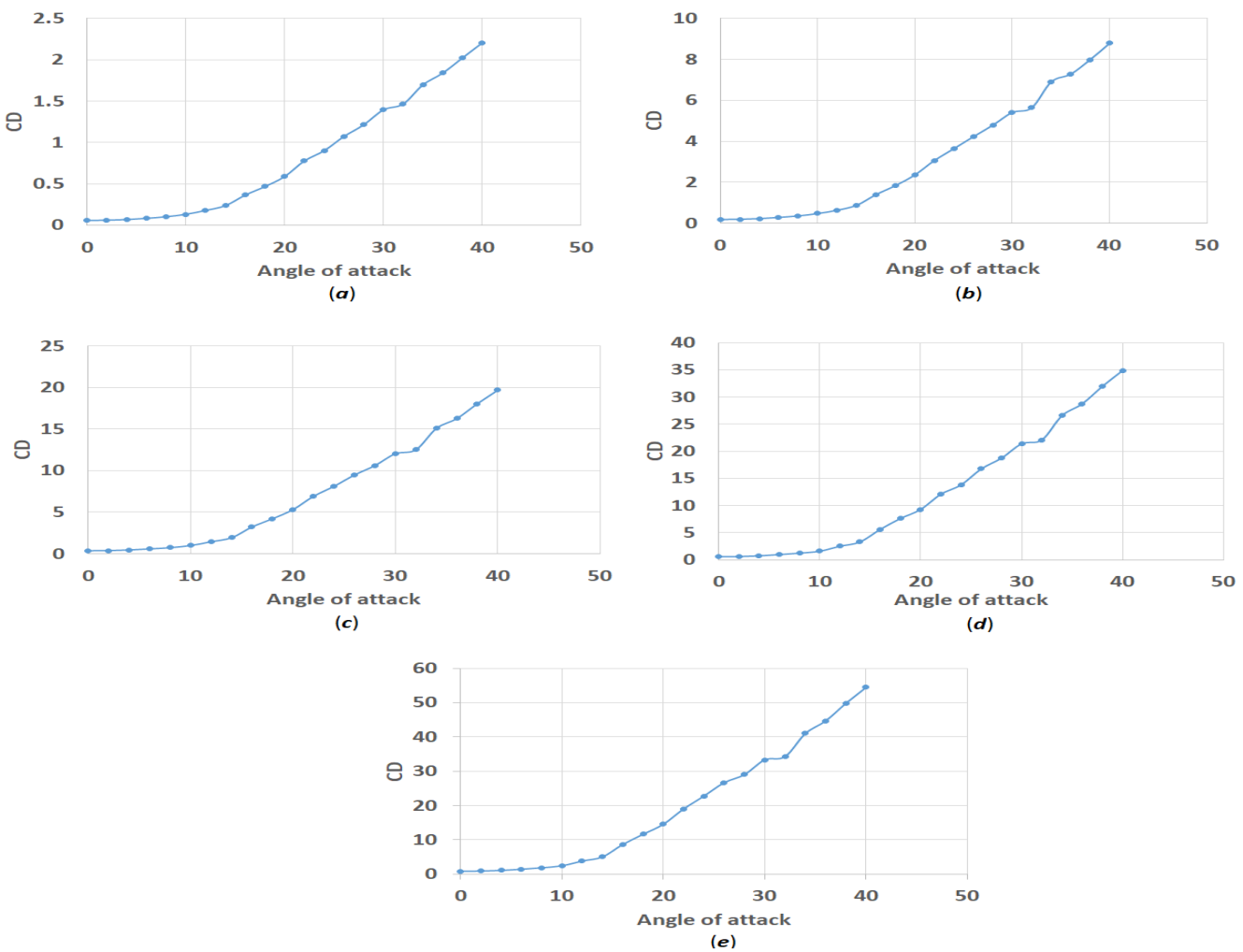


**Fig. 5. Coefficient of drag  $C_D$  against  $\alpha$  for inlet velocity (a)  $u = 2 \text{ m/s}$ , (b)  $u = 4 \text{ m/s}$ , (c)  $u = 6 \text{ m/s}$ , (d)  $u = 8 \text{ m/s}$  and (e)  $u = 10 \text{ m/s}$**

The lift-to-drag ratio (L/D or  $C_L/C_D$ ) evaluates an airplane's aerodynamic performance, as it represents the relationship between the aerodynamic forces of lift and drag. Geodynamicists use the term "lift to drag ratio (L/D or  $C_L/C_D$ )" to quantify this relationship. A high L/D (or  $C_L/C_D$ ) ratio indicates that an airplane has significant lift and minimal drag. In Fig. 6(a), we observe that the ratio  $C_L/C_D$  increases rapidly and reaches to a maximum of 17.2146 against  $\alpha=8^\circ$ . The reason behind this

behavior is the rapid increase in  $C_L$  and the slight increase in  $C_D$  as we have seen in Fig. 4(a) and Fig. 5(a). After  $\alpha=8^\circ$ , the  $C_L/C_D$  curve starts decreasing because there is decline in  $C_L$  and rapid increase in  $C_D$ . Thus  $\alpha=8^\circ$  is the maxima of  $C_L/C_D$  curves for any velocity. After  $\alpha=22^\circ$ , the  $C_L/C_D$  curve flattens and shows an asymptotic behavior. The discussion reveals that the airfoil gives its best performance at  $\alpha=8^\circ$ . A similar pattern is observed in the other graphs of Fig. 6, i.e., Fig. 6 (b), (c), (d), and (e).

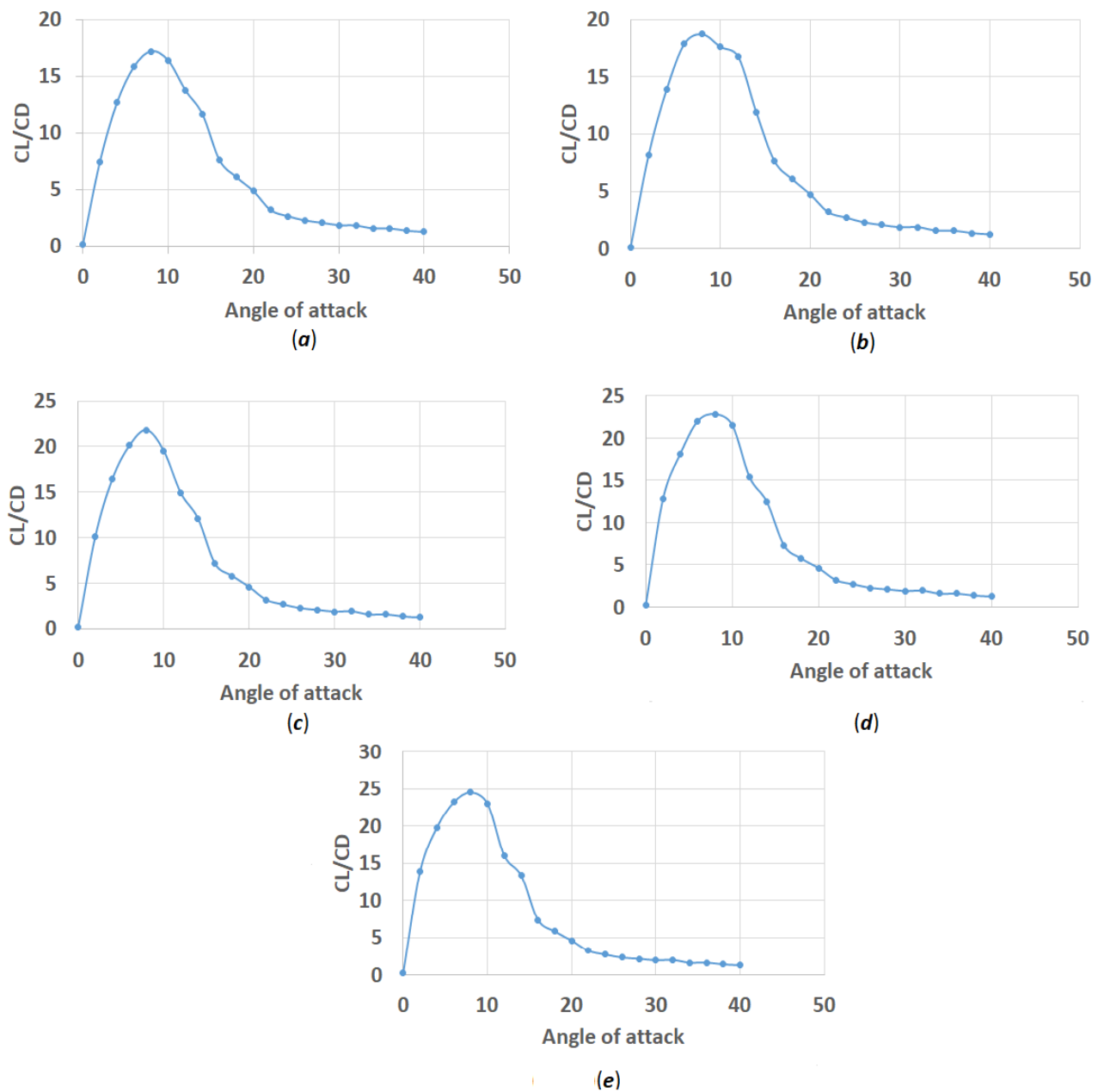


**Fig. 6.  $C_L/C_D$  against  $\alpha$  for inlet velocity (a)  $u = 2 \text{ m/s}$ , (b)  $u = 4 \text{ m/s}$ , (c)  $u = 6 \text{ m/s}$ , (d)  $u = 8 \text{ m/s}$  and (e)  $u = 10 \text{ m/s}$**

In Fig. 7 (a) & (b), the  $C_L$  and  $C_D$  are plotted against inlet velocity at  $\alpha=8^\circ$ . This value  $\alpha=8^\circ$  has been found critical for  $C_L/C_D$  curve. The shape of

both the graphs is parabolic, i.e., both the curves ( $C_L$  and  $C_d$ ) not only rise, but rate of rise also rapid.

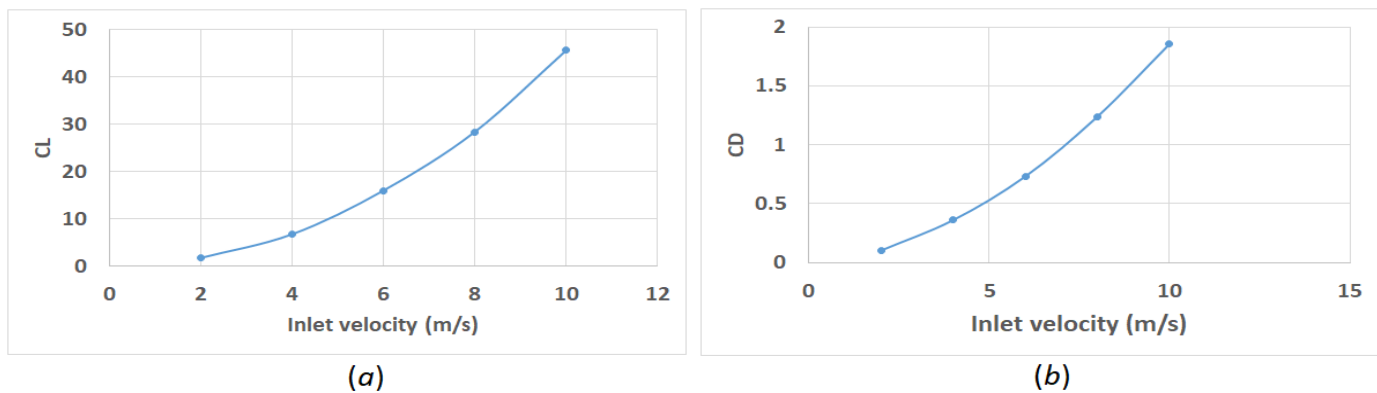
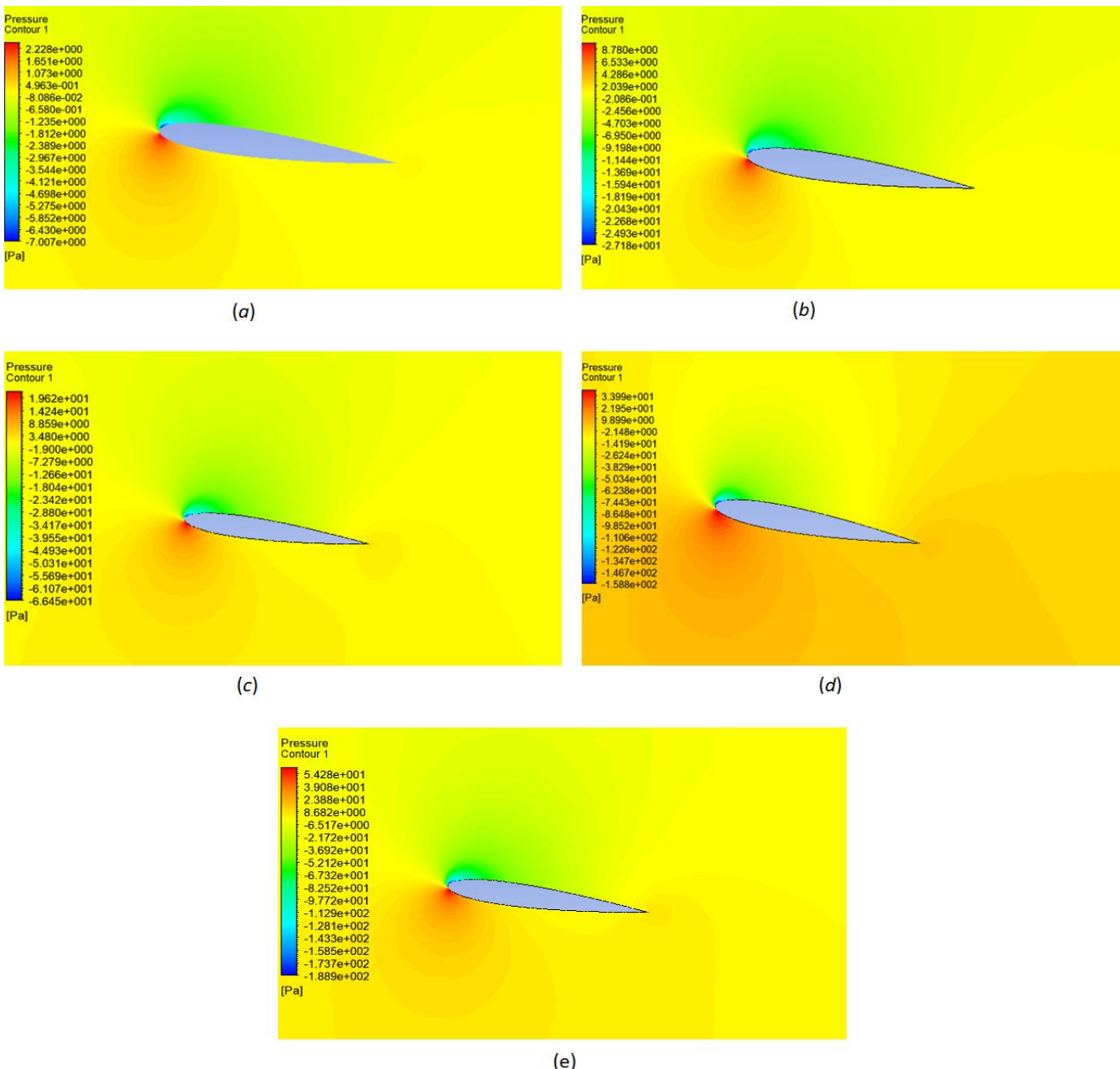


Fig. 7. (a)  $C_L$  against inlet velocity at  $\alpha=8^\circ$ , (b)  $C_D$  against inlet velocity at  $\alpha=8^\circ$ .

To analyze the local aerodynamic behavior against the airfoil, it is important to visualize contours for different parameters. It is important to see the impact of the air pressure on the airfoil. In Fig. 8(a), the contours of static pressure are plotted at  $u = 2$  m/s. We observe that the flow strikes below the leading edge of the airfoil which is called the stagnation point. The gauge pressure at the stagnation point is high that leads the flow stream turn around the airfoil. There is a wake on

the opposite symmetrical position of the airfoil, and the gauge pressure is negative there. The colors of the contours also reveal that the gauge pressure is positive below the airfoil while it is negative above the airfoil. Due to the physics of the problem, flow is supposed to rush towards the wake with a high velocity compared to other locations. This behavior may be seen in Fig. 9(a). The velocity is smaller near the trailing edge also because of the flow separation. A similar pattern is observed for other values of the inlet velocity.



**Fig. 8. Contours of Static Pressure against  $\alpha = 8^0$  for inlet velocity (a)  $u = 2 \text{ m/s}$ , (b)  $u = 4 \text{ m/s}$ , (c)  $u = 6 \text{ m/s}$ , (d)  $u = 8 \text{ m/s}$  and (e)  $u = 10 \text{ m/s}$**

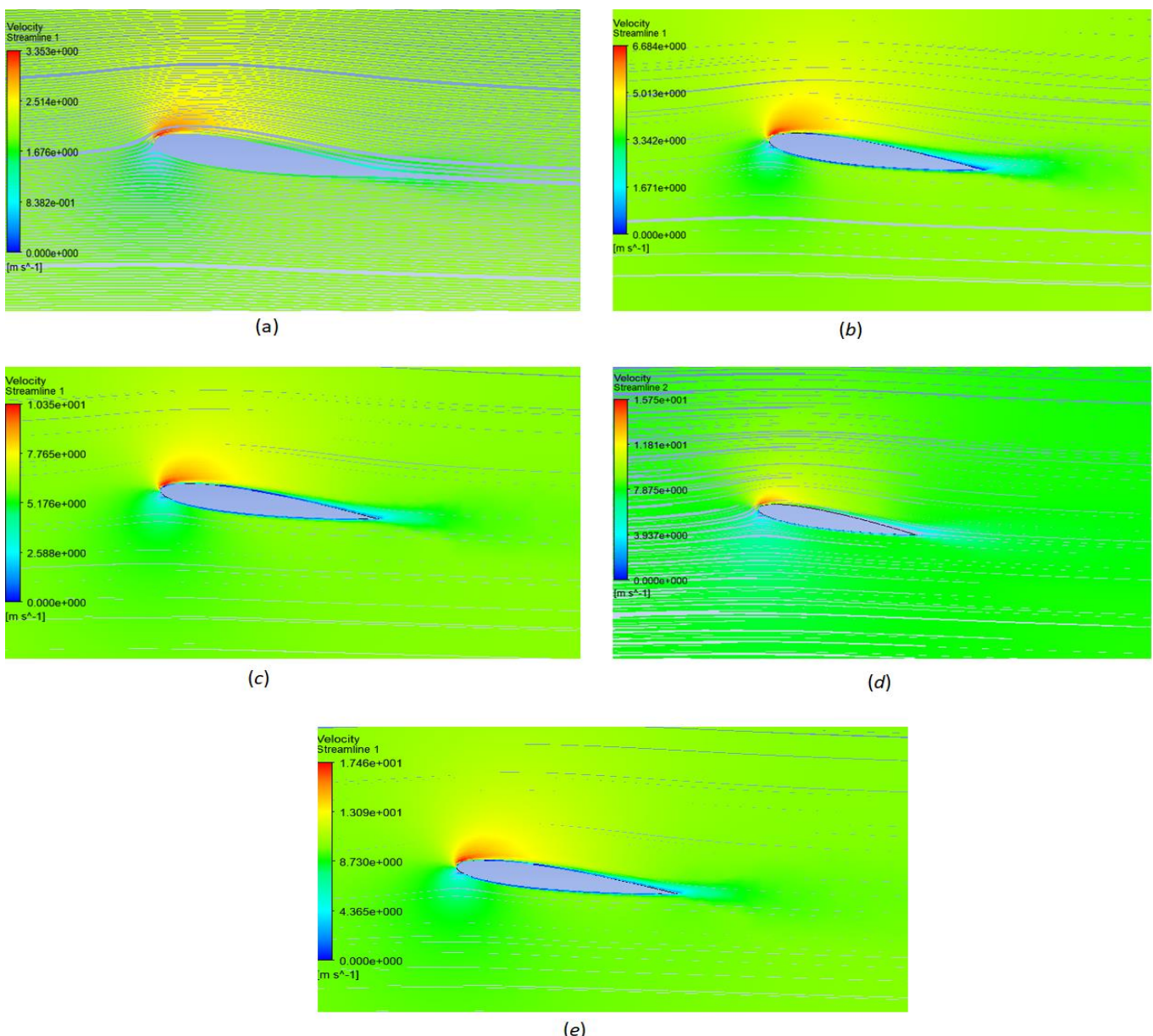


**Fig. 9. Velocity streamlines against  $\alpha = 8^\circ$  for inlet velocity (a)  $u = 2 \text{ m/s}$ , (b)  $u = 4 \text{ m/s}$ , (c)  $u = 6 \text{ m/s}$ , (d)  $u = 8 \text{ m/s}$  and (e)  $u = 10 \text{ m/s}$**

#### 4. Conclusions

This project utilized CFD simulations in ANSYS FLUENT to explore the aerodynamic properties of a NACA 0012 airfoil. By modeling airflow around the airfoil at various angles of attack, our understanding of how these angles influence its behavior has deepened. The simulations for the calculation of lift, drag and their ratio were performed with the following outcomes.

- The  $C_L$  increases from 0 to 2.6 linearly against  $\alpha$  from 0 to  $14^0$  followed by reduction in increase in the  $C_L$ .
- The  $C_D$  increases slightly against the  $\alpha$  from  $0^0$  to  $8^0$ .
- The discussion of  $C_L/C_D$  reveals that the airfoil gives its best performance at  $\alpha=8^0$ .
- The angle of attack  $\alpha=8^0$  has been found to be a maxima for  $C_L/C_D$  curve.
- The  $C_L$  and  $C_D$  exhibit parabolic behavior against the inlet velocity.

#### Bibliography

- [1] Basha, W. Accurate drag prediction for transitional external flow over airfoils. Master's Thesis, Concordia University, Montreal, QC, Canada, 2006.
- [2] Stuck, A.; Turnock, S.; Bress Loff, N. An Evaluation of the RANS Method for the Prediction of Steady Ship Rudder Performance Compared To Wind Tunnel Measurements; Technical Report; University of Southampton: Southampton, UK, 2004.
- [3] Turnock, S.R.; Holroyd, N.J.; Date, J.C. Appendage design for the America's Cup using CFD. In Proceedings of the European Congress on Computational Methods in Applied Sciences and Engineering (ECCOMAS-CFD 2001), Swansea/Wales, UK, 4–7 September 2001.
- [4] Chandrakant Sagat, Pravin Mane and B S Gawali, Experimental and CFD analysis of airfoil at low Reynolds number, International Journal of Mechanical Engineering and Robotics Research, ISSN 2278 – 0149 Vol. 1, No. 3, October 2012
- [5] Wenzinger, C.J.; Harris, T.A. Wind Tunnel Investigation of an NACA 23012 Airfoil with Various Arrangements of Slotted Flaps; Technical Report; NASA: Washington, DC, USA, 1939.
- [6] Todorov, M. Aerodynamic Characteristics of Airfoil with Single Slotted Flap for Light Airplane Wing. In Proceedings of the International Conference of Scientific Paper AFASES 2015, Brasov, Romania, 28–30 May 2015; pp. 509–514.
- [7] Hussein, K.W., Carr, L.W., McCroskey, W.J., 1978, "Dynamic Stall Experiments on the NACA 0012 Airfoil", NASA Technical Paper 1100.
- [8] Hirsch, C. Numerical Computation of Internal and External Flows: Introduction to the Fundamentals of CFD; Butterworth-Heinemann: Oxford, UK, 2007.
- [9] White, F.M. Fluid Mechanics, 8th ed.; McGraw-Hill Education: New York, NY, USA, 2016; pp. 492–499.
- [10] Anderson, J.D. Fundamentals of Aerodynamics, 6th ed.; McGraw-Hill Education: New York, NY, USA, 2017; pp. 567–577.
- [11] Ivan Mary I, Sagaut P, Large Eddy Simulation of Flow Around a High Lift Airfoil. *AIAA Journal*. 2001;8:157-164.
- [12] Richez F, Mary I, Gleize V, Basdevant C. Near stall simulation of the flow around an airfoil using zonal RANS/LES coupling method. *Computers & Fluids*. 2008;37.
- [13] Lehmkuhl O, Baez A, Rodríguez I, P'erez-Segarra CD. Direct Numerical Simulation and Large-eddy Simulations of The Turbulent Flow Around a NACA0012 Airfoil. *7th International Conference on Computational Heat and Mass Transfer*. 2011:1-8.
- [14] Martinat G, Braza M, Hoarau Y, Harran G. Turbulence modeling of the flow past a pitching NACA0012 airfoil at 105 and 106 Reynolds number. *Journal of Fluids and Structures*. 2008;24:1294–1303.
- [15] Kiumars Khani Aminjan. Aerodynamic Analysis of NACA 65-2012 Airfoils at Different Attack Angles with Computational Fluid Dynamics (CFD) Method. *International Journal of*

- Mechanical Handling and Automation.*  
IJMHA. 2018; 4(2):9–16.
- [16] Huang L, Huang PG, LeBeau RP. Numerical study of blowing and suction control mechanism on NACA0012 airfoil. *Journal of Aircraft*. 2004;41:1005-1013.
- [17] Rosas CR. Numerical simulation of flow separation Control by oscillatory fluid injection. PhD Thesis, A&M University, Texas, 2005.
- [18] Beliganur NK, Raymond P. Application of evolutionary algorithms to flow control optimization. Report of University of Kentucky, 2007.
- [19] Bartlett D. W., Patterson Jr J. C., The NASA supercritical-wing technology. CTOL Transport Technol. Conf. (NASA-TM-78731) 1978.